NANO · MICRO small
www.small-journal.com

Photopolymerized Micelle-Laden Hydrogels Can Simultaneously Form and Encapsulate Nanocrystals to Improve Drug Substance Solubility and Expedite Drug Product Design

*Paul Douglas Godfrin, Hyundo Lee, Ji Hyun Lee, and Patrick S. Doyle**

Formulation technologies are critical for increasing the efficacy of drug products containing poorly soluble hydrophobic drugs, which compose roughly 70% of small molecules in commercial pipelines. Nanomedicines, such as nanocrystal formulations and amorphous solid suspensions, are effective approaches to increasing solubility. However, existing techniques require additional processing into a final dosage form, which strongly influences drug delivery and clinical performance. To enhance hydrophobic drug product efficacy and clinical throughput, a hydrogel material is developed as a sacrificial template to simultaneously form and encapsulate nanocrystals. These hydrogels contain micelles chemically bound to the hydrogel matrix, where the surfactant structure dictates the crystal size and drug loading. Therefore, nanocrystals can be produced in high yield (up to 90% drug loading, by weight) with precisely controlled sizes as small as 4 nm independently of hydrogel composition. Nanocrystals and surfactant are then released together to increase the solubility up to 70 times above bulk crystalline material. By integrating nanocrystals into a final dosage form, micelle-laden hydrogels simplify hydrophobic drug product design.

1. Introduction

Nanotechnology can be used in combination with drug substances to design nanomedicines,[1–3] which provide several benefits for drug product performance, including improved bioavailability, biodistribution, and efficacy via targeted delivery.[4–7] A growing impetus for nanomedicines is that 70%–90% of new chemical entities identified by high throughput screening (HTS) technologies for drug discovery are hydrophobic in nature.[8–11] Hydrophobic active pharmaceutical ingredients (APIs) have low solubility that can cause erratic in vitro pharmacokinetic (PK) assay results during early screening.[12] Medicinal chemistry can be used to improve solubility by converting an API to a salt, but many APIs are not compatible with this type of chemical transformation.[13] Therefore, formulation nanotechnologies are a more general and powerful approach to improve the solubility and absorption, distribution, metabolism, and excretion properties of hydrophobic APIs toward improving clinical performance. In contrast, current nanomedicines have primarily focused on targeted delivery (e.g., cellular uptake) of oncology drugs,[14] albeit with slow and expensive development.[15]

Solubility enhancement requires a sensitive balance of API solid state stability and the solubility in aqueous solution. Approaches such as lipid-based systems (such as self-emulsifying drug delivery systems),[16,17] cyclodextrin complexation,[18] and nanovehicles (micelles, liposomes, or dendrimers)[19] improve solubility by introducing a more hydrophobic interface onto which the API partitions in equilibrium with the aqueous solution. However, these co-solutes can hinder API-target binding if partitioning is too effective and also yield low API loading and toxicity concerns due to significant excipient content.[20] Methods such as nanocrystal formation,[4,21–23] amorphous polymer nanoparticles,[24] and porous nanoparticles[5,25] improve the solubility and dissolution rate by stabilizing the API in a state with high surface energy (that depends on API particle size, crystallinity, and polymorph).[26,27]

Of the available formulation nanotechnologies, nanocrystal formation has been the most successful for hydrophobic APIs and is used in several food and drug administration-approved products.[4,21,22] By retaining the crystalline structure, nanocrystals are more stable than amorphous API and are relatively stable to polymorph transformations.[28] Nanocrystals can be synthesized with sizes as small as 100 nm with minimal stabilizer material to limit toxicity and increase drug loading.[4,22,29–31] The large curvature and surface area of nanocrystals provide a driving force for higher solubility (Ostwald–Freundlich equation) and correspondingly faster dissolution (Noyes–Whitney equation) relative to particles on the micrometer scale or larger.[32] In the case of orally delivered nanocrystals, absorption and thus bioavailability are directly correlated with solubility and dissolution rate.[4] An improved dissolution rate also contributes

Dr. P. D. Godfrin, Dr. H. Lee, J. H. Lee, Prof. P. S. Doyle
Department of Chemical Engineering
Massachusetts Institute of Technology
Cambridge, MA 02139, USA
E-mail: pdoyle@mit.edu

The ORCID identification number(s) for the author(s) of this article can be found under https://doi.org/10.1002/smll.201803372.

DOI: 10.1002/smll.201803372

to producing similar absorption and bioavailability in fed and fasted conditions (known as "food effects" due to differences in pH and chemical composition of gastric fluid), which facilitates increased efficacy[29,32,33] and patient compliance.[34,35]

A remaining challenge for drug development is the need to reformulate drug products when transitioning from early to late stage clinical studies. Oral solid dosages (OSDs) are the preferred commercial dosage form due to their excellent patient compliance, API stability and release, reproducibility, and scalability.[34–36] However, current formulation technologies force a compromise between the speed to pivotal first in man studies and the time and cost required to develop a commercial formulation.[37,38] This commonly results in reformulation after phase 1 studies, which is time consuming and resource intensive and could possibly result in failed bioequivalence due to detrimental effects of the OSD formulation and manufacturing process on PK properties.[39,40] In the case of transforming nanocrystal suspensions into OSDs, the added excipients and processing can induce agglomeration, hinder dissolution, or enhance clearance, which can alter the drug release profile and may significantly influence the bioavailability compared to the initial nanocrystal suspension.[41] For nanomedicines to improve clinical performance they require technologies with a more holistic design that can simultaneously comply with the high rate of hydrophobic APIs generated by HTS methods and the requirements of commercially viable final dosage forms.[42,43]

Here, we propose that hydrogels infused with surfactant micelles are a promising technology to improve clinical translation and performance of hydrophobic APIs. Hydrogels are widely used in pharmaceutical formulations due to their biocompatibility and chemical stability, versatility, and responsiveness.[44–48] They begin as solutions (for easy control of dosage form size and shape) that are polymerized into 3D networks of cross-linked hydrophilic polymers with significant pore space.[45,49] The pores can induce and control API crystallization by tuning the geometry and chemistry of the cross-linked matrix.[50,51] This thermodynamically driven process simultaneously encapsulates and stabilizes API, drastically simplifying crystallization and OSD production compared to conventional techniques. By comparison, commonly used top-down techniques for nanocrystal production, such as media milling, jet milling, and high-pressure homogenization, require careful monitoring of the processing conditions to control crystal size and polymorph due to the intense energy input to reduce the size of bulk crystals.[4,22,29–31] Using current techniques, the minimum achievable crystal size is acutely sensitive to the type of stabilizer to prevent polymorph transitions and/or agglomeration.[52,53] The immobilization of nanocrystals within hydrogel pores inherently prevents agglomeration that can occur when nanocrystals are mobile in solution.

Due to the hydrophilicity of hydrogel matrices, loading them with hydrophobic API requires modification to integrate hydrophobic domains within the 3D matrix.[54] The core of surfactant micelles has been used previously to create hydrophobic nanodomains.[55,56] Several studies have modified poloxamer surfactants with acrylate groups to cross-link micelles into hydrogels,[57,58] which can encapsulate and release hydrophobic APIs.[59–62] However, these initial designs of micelle-laden hydrogels never incorporated crystalline API and suffered from restrictively low drug loading and slow release kinetics that limit their utility as OSDs. Release of encapsulated API is controlled by hydrogel network chemistry, which mediates disintegration or swelling to control the mass transport.[45,49] Recent studies have embedded hydrogels with nanocrystals by using nanoemulsions as templates to control crystal size.[63–66] However, limits of emulsion stability prevent completely independent control of drug loading and crystal size.[63] Further, the loss of surfactant during hydrogel cross-linking and API crystallization limits the solubility during drug release.

In this study, micelle-laden hydrogels are used for the first time to template the formation of hydrophobic API nanocrystals to minimize crystal size and maximize API loading, solubility, and release. These hydrogels address many of the obstacles facing the effective development and delivery of hydrophobic APIs. Increasing hydrophobic API solubility is achieved by forming nanocrystals within the micelles and releasing surfactants simultaneously upon delivery. Their capacity for high drug loading, versatile dosage form design, and scalability (from preclinical to commercial scale volumes) can facilitate more successful and efficient clinical translation.

2. Results and Discussion

2.1. Micelle-Laden Hydrogel Synthesis

We have designed a scalable hydrogel-based OSD to facilitate the simultaneous formation and encapsulation of nanocrystalline hydrophobic APIs. Micelles are chemically bound into the hydrogel network, which mechanically stabilizes hydrophobic domains formed by the micelle cores and allows for subsequent chemical and physical manipulation of the composite material without diminishing its ability to encapsulate hydrophobic drugs. As a result, the synthesis, loading, and delivery of this robust system are independent processes, facilitating independent control of hydrogel chemistry and drug crystal loading and size. **Figure 1** demonstrates the sequential steps used to produce micelle-laden hydrogels, including hydrogel dosage form synthesis, loading and crystallization of the hydrophobic API, and drug release.

Micelle-laden hydrogels begin as an aqueous precursor solution consisting of a cross-linking agent (poly(ethylene glycol) diacrylate (PEGDA), M_n = 700 g mol^{-1}), porogen (poly(ethylene glycol) (PEG), M_n = 200 g mol^{-1}), acrylated surfactant, and photoinitiator (PI) (2-hydroxy-2-methylpropiophenone). The spontaneous formation of micelles by surfactants above the critical micelle concentration (CMC) creates hydrophobic nanodomains in which hydrophobic drugs can solidify into nanocrystals. In the absence of co-solvents and co-surfactants, many surfactants can retain the form of a micelle solution up to large concentrations. This provides a framework to integrate a significant quantity of nanodomains with a well-defined, monodisperse size into a given hydrogel. This solution can be handled using a number of solution processing techniques across a wide range of length scales, from microfluidics to yield micrometer-scale particles to casting techniques capable

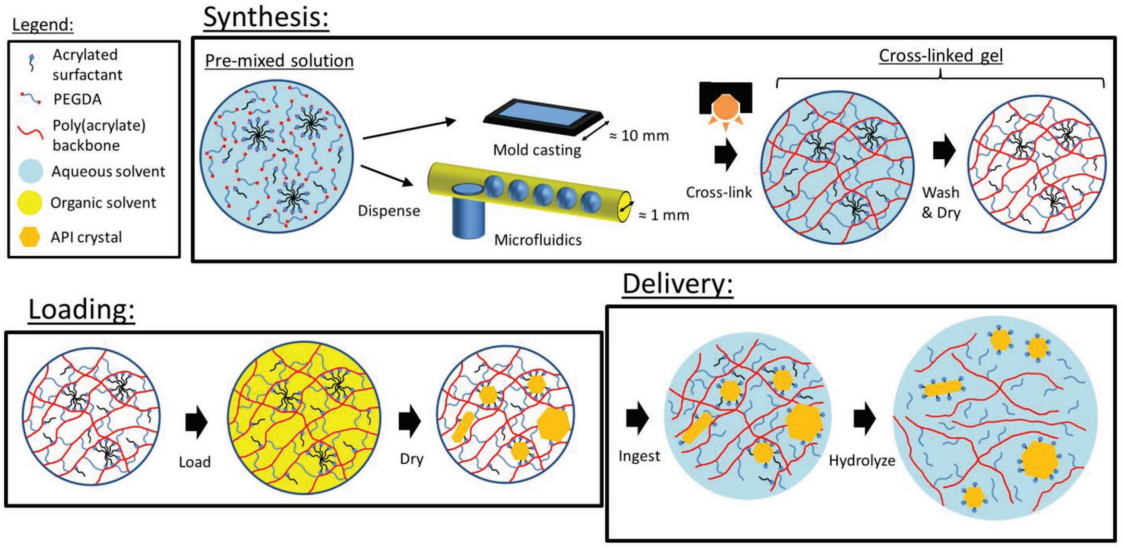

Figure 1. A schematic of the three phases of the micelle-laden hydrogel lifecycle: synthesis, loading, and delivery. During synthesis, a liquid precursor is cast into a preferred form (here either a tablet or a microparticle) and then cross-linked via photoinitiated polymerization and washed to remove unreacted monomers. During loading, the hydrogel is swollen in an organic solvent containing the API, which is then evaporated to induce crystal formation. Finally, delivery of the encapsulated drug occurs when the hydrogel is hydrated, which induces swelling and degradation to release surfactant-stabilized nanocrystals.

of producing tablets or films (schematics of these techniques are provided in Figure 1). Importantly, the number density and size of nanodomains as well as hydrogel chemistry are independent of the dosage form size and shape. In this study, we use a 14 mm (diameter) × 7 mm (height) tablet cast and a microfluidic cross-junction to produce 500 ± 75 µm particles. The hydrogels are then cleaned by soaking them in ethanol to remove PEG, photoinitiator, and unreacted PEGDA and surfactant monomers prior to drug loading.

The purified hydrogel is subsequently loaded with hydrophobic API by soaking it in a suspension of the API in an organic solvent with sufficient time for swelling and homogenous infusion. An ideal solvent has a high saturation concentration of the hydrophobic API, will readily infuse the hydrogel matrix, and is volatile to facilitate low-temperature evaporation. The swollen hydrogel is then removed from the medium before drying to remove solvent, which induces crystallization by supersaturation. Residual solvent content is a concern for OSDs and is quantified using thermal gravimetric analysis (TGA) to reach levels of 1%–2% of the final hydrogel mass. During drying, the temperature is held above the bulk melting temperature of the API, creating a liquid of pure API infused in the mesh. By maintaining the API in its liquid form, it served as a medium to support the hydrogel mesh upon solvent removal and drive heterogeneous nucleation of crystals within the mesh rather than on the surface. Upon cooling, crystallization occurs within the hydrophobic cores of the micelles or the pores of the hydrogel mesh. Thus, the distribution of crystal sizes will depend on the exact hydrogel composition. The nanocrystals formed in either environment of micelle-laden hydrogels are stabilized from coalescence and degradation due to physical separation from each other and the environment. While this protocol leaves behind some API, future iterations will optimize this process to achieve 100% encapsulation efficiency by using containers designed to localize API solution within the hydrogels during the drying process.

In this work, fenofibrate (FEN) is used as a canonical hydrophobic API based on its availability and extensive use in prior studies. In particular, recent work has quantified the relationship between crystalline FEN melting point and crystal size by using porous glass beads with varying pore sizes,[25] which will be utilized as a calibration curve to quantify crystal size distributions within micelle-laden hydrogels using dynamic scanning calorimetry (DSC). To demonstrate the general applicability of micelle-laden hydrogels to poorly soluble APIs, we also provide preliminary evidence of nanocrystal formulation using ibuprofen in the Supporting Information. However, a more comprehensive demonstration of micelle-laden hydrogel performance is the focus of ongoing research.

When the hydrogel is rehydrated in aqueous solution, it swells and is hydrolyzed, releasing the API. In the latter case, the matrix simultaneously releases surfactant that increases the solubility of the hydrophobic drug, enhances the kinetics of dissolution, and prevents supersaturation and recrystallization. Due to the chemical modifications that occur during hydrogel synthesis (radical polymerization) and degradation (hydrolysis), the material released during drug delivery is distinct from the initial reactants. For the PEGDA-based gels used here, the hydrolysis products include PEG and partially cross-linked polyacrylates (e.g., Eudragit and Carbopol), which are both widely used excipients. The degradation can also be leveraged to convert an OSD vehicle to a liquid formulation for preclinical studies.[67]

In order to explore the effect of surfactant properties on nanocrystal formation, a range of alkyl ethoxy and poloxamer surfactants are integrated into hydrogel matrices. **Table 1** outlines the surfactants studied, which vary in the length of the hydrophobic and hydrophilic units. The alpha numeric names

Table 1. Summary of chemical properties of the surfactants used in this study, including molecular weight (M_n), HLB value, critical micelle concentration (CMC), and chemical composition of the original surfactants and hydrodynamic diameter before (D_h) and after (aD_h) the acrylation reaction and corresponding standard deviations.

Surfactant	M_n	HLB	CMC [% w/v]	# C/PPG	# PEG	D_h [nm]	aD_h [nm]
L10	627	13.6	9×10^{-3}	12	10	8.4 ± 0.5	10.5 ± 0.3
C10	683	12.9	1×10^{-4}	16	10	23.5 ± 1.5	12.6 ± 0.8
L23	1268	16.9	8×10^{-3}	12	23	8.6 ± 0.2	8.7 ± 0.1
C20	1124	15.7	8×10^{-4}	16	20	10.1 ± 0.1	10.2 ± 0.1
S20	1152	15.3	7×10^{-4}	18	20	11.2 ± 0.4	16.0 ± 0.4
B25	1496	17.3	–	22	25	–	12.8 ± 0.1
S100	4738	18.8	1×10^{-2}	18	100	24.9 ± 1.3	26.1 ± 0.8
F68	8400	>24	4×10^{-1}	30	80	7.1 ± 0.2	12.5 ± 0.4
F127	12 700	22	4×10^{-2}	70	106	8.9 ± 0.9	9.4 ± 0.4

refer first to the alkyl chain (L = lauryl, C = cetyl, S = stearyl, and B = behenyl) and second to the PEG length in the number of monomeric units. The two poloxamer triblock surfactants studied are F68 and F127, which contain a polypropylene glycol (PPG) hydrophobic region rather than an alkyl chain. The surfactants are organized into three sub-sections distinguished by the size of the PEG region, which correspond to roughly 10, 20, and 100 PEG units. Thus, the influence of the size of the PEG segment and hydrophobic core of the micelle can be independently studied.

Integrating micelle templated hydrophobic domains into hydrogel matrices requires that the surfactants are capable of being chemically bonded to the matrix. A variety of functional groups can be used, but here we add an acrylate group to the hydrophilic end of the surfactant, as done previously,[57,61] for its compatibility with PEGDA-based hydrogels. One exception is surfactant B25, which was purchased in the acrylated form. Dynamic light scattering (DLS) confirms that the surfactants remain water soluble and form micelles of similar diameter (see Table 1) after acquiring an acrylate group. Fourier-transform infrared (FTIR) spectra (shown in the Supporting Information) replicate prior work[61] and demonstrate the loss of the IR band (3500 cm^{-1}) from hydroxyl groups initially present and the evolution of bands (1640 and 1720 cm^{-1}) corresponding to acrylate functional groups after the reaction with acryloyl chloride.

2.2. Characterization of Crystal Size Distributions within Hydrogels

As with prior work utilizing hydrogels to encapsulate API crystals,[50,51] the significant void space of the matrix scaffold creates domains within which crystallization can take place. Therefore, the PEGDA matrices that will later serve as the scaffold for acrylated micelles will themselves template crystals. Although the presence of surfactant, even not in micellar form, will alter crystallization in the mesh, quantifying the relationship between the matrix composition and crystal size will set the foundation for identifying the effect of micellar domains.

A range of PEGDA and PEG porogen volume fractions are studied to correlate the network structure and composition with the corresponding crystal size distributions and drug loading. Prior work has demonstrated that the equilibrium swelling (and thus, the mesh size) of PEGDA hydrogels decreases as PEGDA content increases, due to shorter spacing between cross-links, and increases with PEG content, due to its excluded volume.[45] These features will play a role in the resulting crystal size distribution formed by the encapsulated API, but will not correlate directly. Following our API loading protocol, the hydrogels are not in an equilibrium swollen state prior to crystallization due solvent removal, which precludes the use of equilibrium swelling models to quantify the mesh size in which crystals form. Further, the mesh size (when infused liquid API) is likely to be subsequently distorted during crystallization. Network segments will be more coiled in a less swollen state and thus have more flexibility to self-associate due to the contrast in hydrophobicity of the API and the hydrogel matrix. Further, PEG and polyacrylate segments are also expected to be expelled from the crystallization front of the hydrophobic API. Thus, the final crystal size distribution and API loading will be sensitive to the initial mesh size as well as the thermodynamic driving forces for self-association of the hydrogel network segments during crystallization, which require direct measurement under each condition.

The extent of crystallization within hydrogels was determined by DSC, which can quantify the content and size of crystals according to the known shift in melting point and enthalpy of melting as a function of crystal size.[68] For example, bulk fenofibrate displays a prominent peak near the melting temperature of 81 °C, while drug-loaded hydrogels have a peak that is shifted to lower temperatures. All peaks are confirmed to correspond to crystalline fenofibrate by the formation of peaks in X-ray powder diffraction data (provided in the Supporting Information) and the lack of any exothermic (positive specific heat flow) signal in the DSC curves, which would indicate crystallization of amorphous fenofibrate during the experiment. The theory and fitting protocol are described in detail in the Supporting Information. By fitting DSC thermograms, the cumulative crystal size distribution, $C(D)$, is extracted, which indicates the mass fraction of crystals that are equal to or smaller than a particular size. Raw DSC results for all hydrogel compositions studied here are provided in the Supporting Information, as all results moving forward will be presented in the form of $C(D)$.

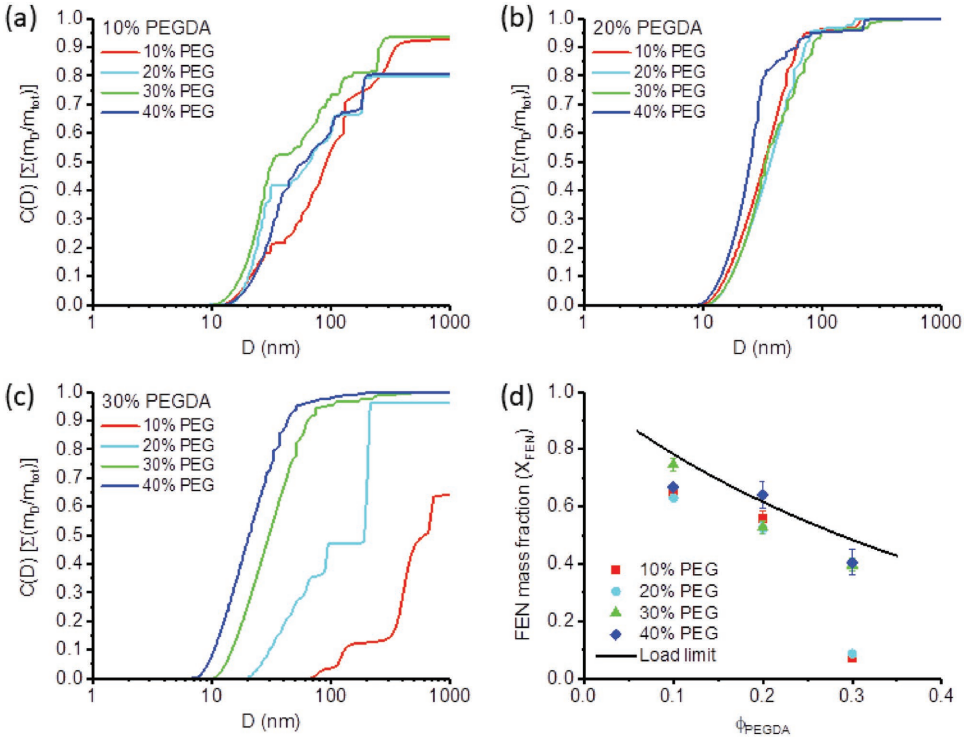

Figure 2. Cumulative crystal size distributions are provided for hydrogel compositions with a) 10%, b) 20%, and c) 30% PEGDA and a range of PEG volume fractions. d) Fenofibrate mass fractions in hydrogels without surfactant are plotted as a function of PEGDA volume fraction for several PEG volume fractions. The theoretical drug loading limit is plotted for the fenofibrate solution used to load hydrogels (450 mg mL^{-1}, black solid line).

Figure 2 shows the full set of $C(D)$ functions extracted from the DSC thermograms of "plain" PEGDA-based hydrogels (without surfactant) loaded with fenofibrate and the corresponding weight fraction of API loaded in the hydrogels. The $C(D)$ plots are restricted to crystal sizes below 1000 nm given that crystals of this size and larger are representative of bulk fenofibrate (see the Supporting Information) and therefore not all $C(D)$ functions reach a value of one within this size range. At the smallest PEGDA content (10% by volume), 20%–30% of crystals are 200 nm or larger in size. The remaining crystals fall within a broad distribution of sizes ranging from 20 to 200 nm. For comparison, current commercial methods for nanocrystal formation can only reach a minimum crystal size on the order of 100 nm.[30,63] As the PEGDA content is increased to 20% by volume, the crystal size distribution becomes more monodisperse around sizes ranging from 30 to 50 nm for all PEG concentrations with no bulk crystals detected. At this cross-linker concentration, PEG content has a minimal effect on $C(D)$. At 30% PEGDA, PEG content has a strong impact on the distribution of crystal sizes. The hydrogels with 10% and 20% PEG only show signs of bulk and roughly 200 nm (and larger) crystal formation. When the PEG content is increased to 30% and 40% by volume, crystal sizes shift to a range of 10–40 nm.

The $C(D)$ quantified in each hydrogel can be understood in terms of the crystallization process relative to the hydrogel microstructure. Figure 2 demonstrates that the $C(D)$ for hydrogels with 10% PEGDA are significantly more polydisperse than those with 20% PEGDA and generally form larger crystals. The smaller crystal sizes formed in hydrogels with 20% PEGDA relative to 10% PEGDA correlate with a smaller average pore size known to result from the higher cross-linking density.[45] More cross-links also limit configurational rearrangement during crystallization and create a much less polydisperse $C(D)$ for 20% PEGDA hydrogels. The larger variability in the effect of PEG content on $C(D)$ in 10% PEGDA hydrogels is hypothesized to result from the higher chemical flexibility in the more open matrix structure with lower cross-linking density. Thus, the crystal size distribution becomes more polydisperse due to the larger free volume for structural rearrangement (drive by matrix self-association in a highly hydrophobic environment) in 10% PEGDA hydrogels.

At 30% PEGDA, where the cross-linking density is even higher, the mesh size sets a physical limit for nanocrystal formation and encapsulation. Although not shown by $C(D)$, the peaks in DSC thermograms of hydrogels with 30% PEGDA and 10% or 20% PEG are very weak (see the Supporting Information). Figure 2d shows that these hydrogels have very low drug loading, generated by integrating DSC thermograms as a function of hydrogel composition. As a side note, drug loading measured by DSC integration is quantitatively consistent with direct measurement by TGA (shown in the Supporting Information). By comparing drug loading in hydrogels to an estimate assuming the hydrogel volume remains constant (black line in Figure 2d), the extent of swelling can be indirectly quantified. That a majority of hydrogel compositions closely follow the loading estimate indicates that the hydrogels roughly remain swollen to the initial volume after introducing API in organic solvent. However, the reduced loading in hydrogels at 30%

PEGDA with 10% and 20% PEG results from the high cross-linking density. Thus, a minimum amount of PEG porogen is necessary to create pores large enough to facilitate API loading. Specifically, PEG segments are in close enough proximity for widespread self-association during crystallization (where organic solvent is removed and only pure liquid and highly hydrophobic FEN remains) such that the hydrogel deswells and reduces the volume of pores within which API can crystallize. However, the remaining pores are large enough to facilitate nucleation and growth of FEN crystals as seen in the $C(D)$.

These results indicate that PEGDA hydrogels can facilitate the formation of a range of hydrophobic API nanocrystal sizes as low as 10 nm. However, similar to amorphous solid dispersions, these nanocrystals would quickly reach supersaturation when released into aqueous solution in the absence of a solubility enhancer. We use prior work with micellar solutions as a precedent to improve solubility, but now integrate micelles into these hydrogels with biodegradable functional groups to further reduce the crystal sizes and improve the solubility upon release. In the following sections, we explore the effects of incorporating surfactants into PEGDA hydrogels that may influence micelle self-assembly and stability. Further, the matrix may indirectly influence the micelle size and structure if there is a size mismatch with the mesh that may either constrict or stretch the internal hydrophobic domain. Therefore, it is necessary to investigate a range of hydrogel compositions to quantify the ability of micelle-laden hydrogels to template nanocrystal formation.

2.3. Effect of Surfactant Concentration on Nanocrystal Formation

An optimal micelle laden hydrogel formulation would yield high loading of API nanocrystals with minimal surfactant content. The critical micelle concentration of the surfactants used here is all on the order of 10×10^{-6} M (see Table 1), providing a small barrier to the formation of micelles. However, given that pores within the hydrogel mesh serve as nucleation centers, a critical density of micelle domains will be necessary to drive crystallization to preferentially occur within these hydrophobic domains. In the other extreme, at high surfactant concentrations, surfactants may self-assemble into larger length scale structures, such as sheets or ordered cubic phases.[69] As a result, we study a range of concentrations for a subset of surfactants in one matrix composition to identify these possible outcomes.

The effects of surfactant concentration and hydrophobic segment size are tested by comparing three surfactants (L23, S20, and B25) with similar PEG lengths and three concentrations (4.2, 8.4, and 12.6% w/v) in a hydrogel matrix composed of 20% PEGDA with 20% PEG. The corresponding cumulative crystal size distributions are provided in **Figure 3**. Under nearly all conditions with surfactant, the $C(D)$ functions are shifted to include smaller crystals than the "plain" hydrogels. Surfactants S20 and B25 produce crystals below 10 nm, which do not appear in "plain" hydrogels and are similar in size to micelles (see Table 1) and are therefore labeled as

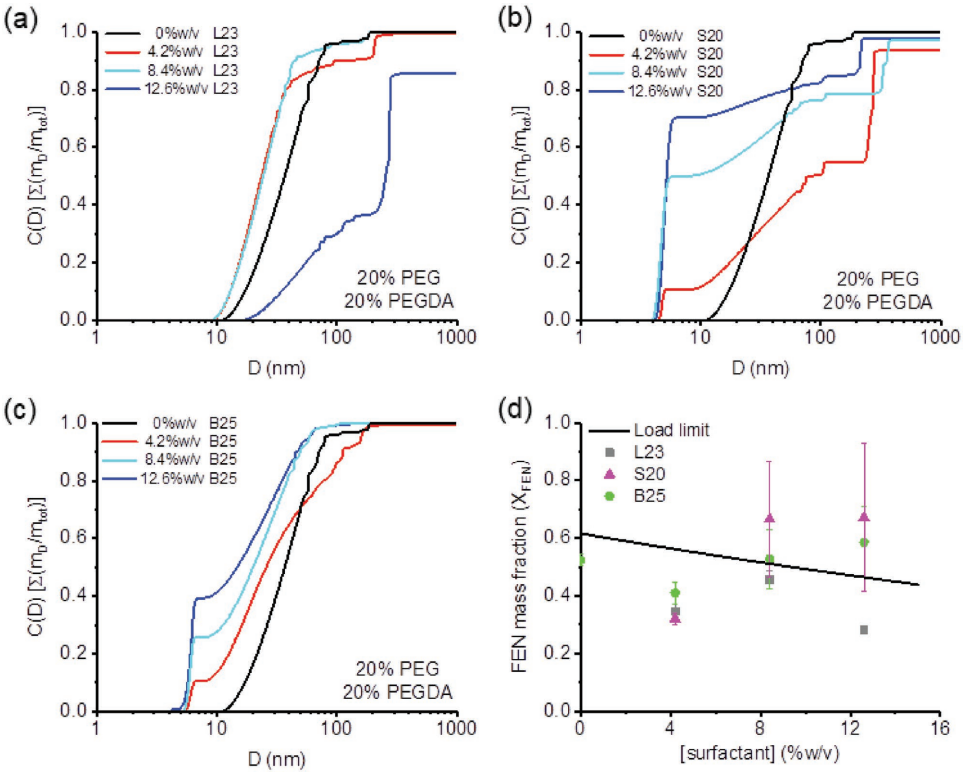

Figure 3. Cumulative crystal size distributions for hydrogels with 20% PEGDA and 20% PEG and surfactants a) L23, b) B25, and c) S20 at three concentrations. d) The fenofibrate loading (by weight), determined by integrating DSC thermogram curves, is plotted for each hydrogel composition. Also shown are the theoretical limits when loading the hydrogels from a 450 mg mL^{-1} solution (black line).

micelle-templated nanocrystals (MTNs). For both surfactants, the relative content of MTNs scales directly with surfactant concentration and thus the density of micelles (all concentrations are well above the CMC). In the case of S20, the surfactant also creates a larger content of 200–400 nm crystals relative to the "plain" hydrogel. Surfactant L23 is unable to produce MTNs and, at the highest surfactant concentration, these hydrogels contain significantly larger crystals than the corresponding "plain" hydrogel. The lack of MTNs formed by L23 suggests that this (12 carbon) alkyl chain length forms too small of a hydrophobic domain to nucleate crystals, in contrast to the larger hydrophobic components of S20 (18 carbons) and B25 (22 carbons) that readily template crystals below 10 nm in size.

Surfactant concentration also influences drug loading, as demonstrated in Figure 3d. Interestingly, API loading in hydrogels with 4.2% w/v of all surfactants is lower than the "plain" hydrogel. At this concentration, loading is also lower than expected assuming the hydrogel volume remains constant (solid line in Figure 3d). However, API loading in micelle-laden hydrogels generally increases with surfactant concentration (L23 hydrogels are an exception). Given the finite volume of the PEGDA and surfactant, the observed increase in API mass fraction with increasing surfactant concentration indicates that the addition of surfactant increases the hydrophobicity of the matrix and enhances the swelling of the hydrogels during drug loading. Thus, additional API can infuse the extra volume from enhanced swelling and increases the final drug loading at higher surfactant concentration.

These crystal size and drug loading trends result from the equilibrium of surfactant monomers and micelles in solution and their subsequent self-association. Similar to the "plain" 30% PEGDA hydrogels with 10% PEG, L23 hydrogels that form an excess of 200 nm crystals correspond with low drug loading. This behavior and the lack of MTNs formed by L23 suggest that its 12 carbon alkyl chain preferentially self-associates rather than interacting with fenofibrate. This effect increases with surfactant concentration until, at 12.3% w/v L23, widespread surfactant self-association causes the hydrogel to contract (reducing the API loading) and creates large pores by distorting the hydrogel mesh (creating larger crystals). In contrast, S20 and B25 readily associate with fenofibrate to facilitate nucleation and stabilization of MTNs within their hydrophobic micelle cores. The formation of 200 nm crystals in the $C(D)$ of S20, which the "plain" hydrogel does not form, indicates that S20 monomers cause an increase in the size of matrix pores, within which API crystallizes. The increase in API loading due to swelling of S20 hydrogels suggests that the stearyl (18 carbon) chains preferentially self-associate and distort the matrix pores. Thus, surfactants with longer hydrophobic segments favor interactions with API to form MTNs rather than self-associations that manipulate the matrix. However, the local minimum in API loading at 4.2% w/v surfactant suggests that a minimum surfactant concentration is necessary to retain a significant content of micelle structures within the matrix (as opposed to larger hydrophobic domains). Moving forward, a surfactant concentration of 8.4% w/v will be used to maximize MTN formation and API loading, but limit the surfactant concentration and the content of crystals larger than 100 nm.

2.4. Effect of Surfactant Chemistry on Nanocrystal Formation

To further generalize the limits of MTN formation in micelle-laden hydrogels, the surfactant PEG segment size and hydrogel PEGDA content are also varied. Each of the surfactants listed in Table 1 is formulated (at 8.4% w/v) with 10%, 20%, and 30% PEGDA with 20% PEG as a porogen. The variation in matrix composition provides a range of mesh sizes to observe the influence of the hydrogel scaffold on micelle templating. The $C(D)$ functions as well as drug loading extracted from DSC thermograms are shown in **Figure 4** for all hydrogel compositions tested.

In almost all hydrogel compositions, the presence of micelles reduces the population of bulk and matrix-size crystals. Depending on the composition, micelle-laden hydrogels can incorporate between 15% and 50% of the encapsulated API in the form of MTNs. Only surfactants L10, L23, and C20 were unable to form MTNs under all matrix conditions. Hydrogels with L10 and L23 had similar $C(D)$ functions to the corresponding "plain" hydrogel while those with C20 created much larger crystals, which is thought to arise from significant self-association. These results again demonstrate that surfactants with a lauryl (12 carbon) alkyl chain have too small of a hydrophobic segment to form MTNs. Given that the C10 surfactant forms MTNs, it is determined that a cetyl (16 carbon) segment is a lower limit of alkyl chain length for MTN formation within micelle-laden hydrogels.

All crystals other than MTNs are similar in size to those found in the corresponding "plain" hydrogel, but with a smaller population. Only in 20% PEGDA hydrogels did the "small" surfactants (C10 and S20) produce crystals that were larger in size than those formed without surfactant present. This can be attributed to a balance of close proximity for surfactant monomers to self-associate (pores in 10% PEGDA are too large) and sufficient space for that association to constrict the matrix (pores in 30% PEGDA are already very small). At 20% and 30% PEGDA, the "large" surfactants (B25, S100, F68, and F127) significantly shift the $C(D)$ to crystal sizes below those formed by the corresponding "plain" hydrogels. This is exemplified best in the hydrogels with 30% PEGDA (see Figure 4c).

The size of MTNs formed in micelle-laden hydrogels is a direct function of micelle size. **Figure 5**a shows the MTN size normalized by the hydrodynamic diameter of the micelle for all surfactants that yield MTNs. Under all conditions, the hydrodynamic diameter of the micelles sets an upper limit for nanocrystal size. That the final crystal size is always smaller than the templating micelle reflects the fact that the internal hydrophobic corona is only a fraction of the total volume of the micelle. The value of $D_{crystal}/D_{micelle}$ varies in proportion to the micelle diameter and hydrophobic segment length (see Table 1) and the density of the hydrophobic segment (PPG is more dense than alkanes, providing more volume for crystal growth). This is explicitly demonstrated in Figure 5b, where the MTN size in each micelle-laden hydrogel composition is found to correlate linearly with the surfactant hydrophilic-lipophilic balance (HLB). Thus, more hydrophobic surfactants (lower HLB) can facilitate smaller MTNs of hydrophobic API, with a lower limit near 13 corresponding to the transition from oil in water to water in oil stabilizing surfactants.

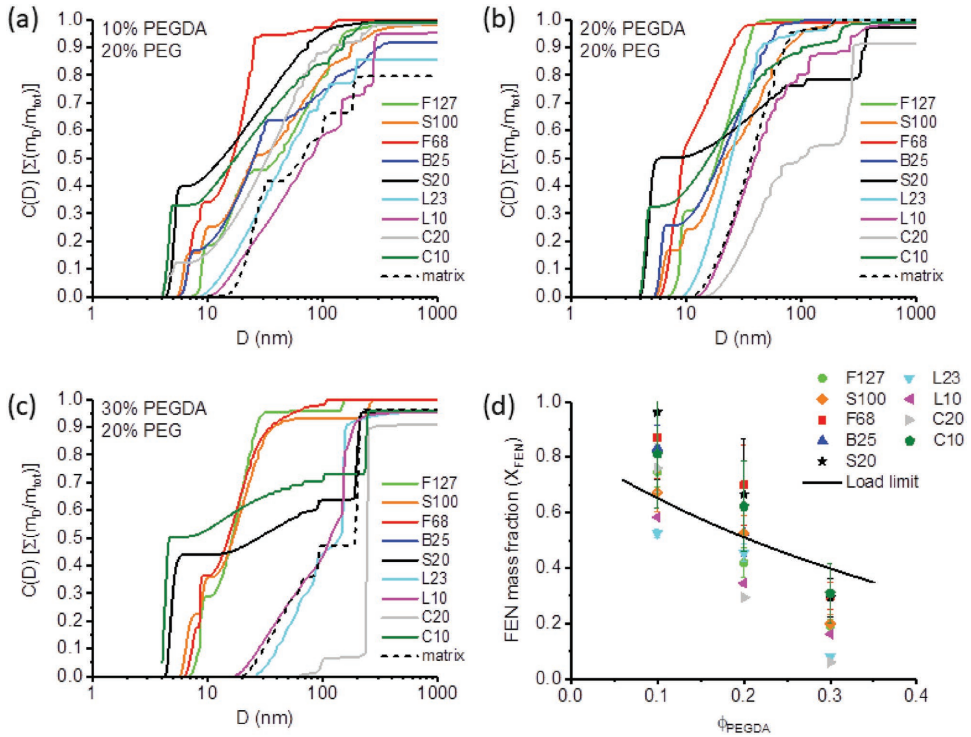

Figure 4. Cumulative crystal size distributions of FEN-loaded micelle-laden hydrogels with surfactants in Table 1 at a concentration of 8.4% w/v embedded in a) 10%, b) 20%, and c) 30% PEGDA with 20% PEG porogen. d) Drug loading (as weight fraction) is quantified by integrating DSC thermograms and plotted as a function of PEGDA concentration relative to the maximum assuming no hydrogel swelling (solid line).

Importantly, the hydrogel matrix composition does not appear to influence the size of crystals formed within micelles (no change in $D_{crystal}/D_{micelle}$ across PEGDA concentrations). The implications of this behavior are profound for the capability of this platform material to orthogonally tune the gel and API properties. This result is particularly interesting given that hydrogels composed of 30% PEGDA and 20% PEG without surfactant were unable to facilitate any appreciable fenofibrate loading (see Figure 2d). The consistency of crystal to micelle size ratios is believed to arise from the capability of the PEG segments to rearrange during the solvent removal process of crystallization. The PEG acts as a buffer, allowing the hydrophobic core to template crystallization regardless of the micelle's surroundings. As a result, the organic solvent and drug concentration are expected to influence the crystal size formed within micelles.

The extent of drug loading is shown in Figure 4d. The drug loading depends on the PEGDA and surfactant concentrations, but those with MTNs always improve loading. Thus, the presence of surfactants is not sufficient to improve loading, but that they subsequently induce MTN formation. Surfactants that do not form MTNs do so as a result of self-association that also restricts hydrogel swelling. When the matrix is immersed in the hydrophobic organic solvent with API during drug loading, the surfactants that preferentially associate with FEN cause the hydrogel to swell and increase these favorable interactions. This increased uptake of solvent increases the hydrogel volume above its original state and leads to drug loading values that exceed estimates assuming a constant volume (black line in Figure 4d). In the case of 10% PEGDA hydrogels with S20, API loading exceeds 90% by weight, which is a significant enhancement relative to techniques currently used in industry.[4,30]

The influence of forming MTNs on drug loading is highlighted in Figure 5c, which demonstrates that total drug loading in hydrogels with a set PEGDA concentration correlates linearly with the content of MTNs. Deviations in MTN content (despite the constant surfactant concentration) arise from the matrix flexibility and cross-linking density, which influence the proximity of individual surfactant molecules to self-associate and maintain the hydrophobic nanodomain structure. For example, 10% PEGDA hydrogels contain less MTNs due to a more open network structure while an equivalent content of MTNs in hydrogels with 30% PEGDA is unable to improve loading relative to those with 20% PEGDA due to a restrictively high cross-linking density that limits swelling. Thus, the relative fraction of MTNs results from a combination of the PEGDA content and surfactant HLB. However, the hydrogels with the highest API loading are not necessarily those with the most MTNs. Thus, achieving high loading of minimal crystal size is a matter of optimizing the concentrations of surfactant and PEGDA.

2.5. Characterization of Solubility Enhancement by Micelle-Laden Hydrogels

The efficacy of hydrophobic APIs loaded in micelle-laden hydrogels as an OSD depends on the solubility enhancement and dissolution kinetics after release. **Figure 6**a provides a schematic

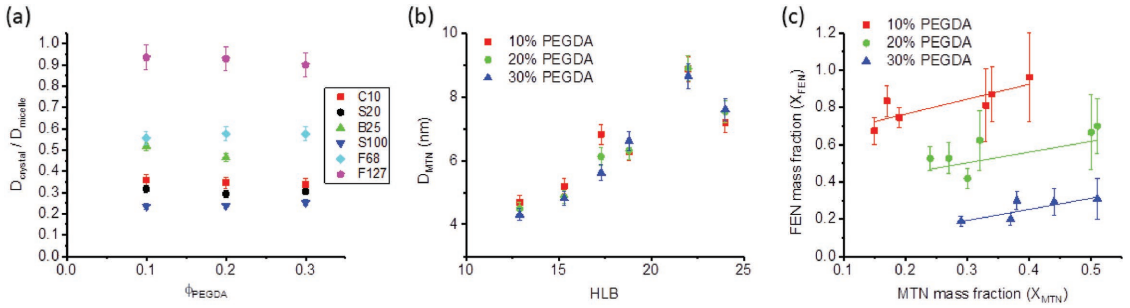

Figure 5. a) The ratio of the MTN crystal size to the micelle hydrodynamic diameter is plotted as a function of hydrogel PEGDA content (all with 20% PEG porogen). Surfactants that did not form nanocrystals under all conditions were not included. b) The MTN crystal diameter is plotted as a function of HLB to demonstrate the linear correlation of the two. c) The total FEN mass fraction in hydrogels (X_{FEN}) is plotted for each PEGDA concentration as a function of the mass fraction of FEN in the form of MTNs (X_{MTN}), which also show linear correlations (the lines are linear fits).

of the two mass transport mechanisms that contribute to drug delivery. When hydrated, both the swelling and hydrolysis of the matrix will influence the API release,[45] and the occurrence of each mechanism will depend on the physiological conditions. Thus, we control the solution conditions of in vitro dissolution by varying the pH of the dissolution media to restrict API release to one mechanism at a time (either swelling/diffusion or decomposition). API release by hydrogel decomposition will demonstrate the maximum achievable drug release in saturated conditions and quantify the solubility enhancement by MTNs in micelle-laden hydrogels. API release by diffusion will demonstrate the increase in dissolution rate provided by the formation of MTNs. We note that our aim is to demonstrate the improvement in dissolution from micelle-laden hydrogels due to MTN formation rather than complete control of release kinetics, which depends on matrix composition and dosage form size/shape. While the PEGDA cross-linker used here does not decompose in physiologically relevant solutions, the design of rapidly hydrolyzing cross-linkers that do is the focus of ongoing research.

The release of fenofibrate by decomposition of micelle-laden hydrogels in saturated conditions is conducted by dispersing tablets in an alkaline sodium hydroxide solution (1.0 M) without additional surfactant. These solution conditions are required to hydrolyze the ester groups of the PEGDA and surfactant, which allows the encapsulated crystals, surfactant, and PEG to be released. Here, the surfactant content of the hydrogels is only sufficient to solvate up to 2 μg mL^{-1} based on an equivalent solubility enhancement of the surfactants used here to that measured for sodium dodecyl sulfate (SDS).[70,71] Further, nanoscale crystals are only estimated to increase solubility by about 65% at best, according to the Ostwald–Freundlich equation (shown in the Supporting Information). However, UV–vis measurements of decomposed hydrogel samples demonstrate that the micelle-laden hydrogels achieve concentrations of roughly 40 μg mL^{-1}, as shown in Figure 6b. Thus, the release of drug nanocrystals and surfactant yields an aqueous suspension with a concentration up to 70 times that of bulk fenofibrate in an equivalent surfactant solution.

The drastically higher solubility after release from the micelle-laden hydrogels is facilitated by the presence of nanocrystals and the stabilization of crystal surfaces by the surfactant. Solubility enhancement by micelles results from the association of individual drug molecules in the micelle core and/or at the hydrophobic/hydrophilic interface. While nanoscale micelles have a large surface area, most of the volume is consumed by the surfactant itself, leaving minimal space to solubilize the API. In contrast, micelle-laden hydrogels form nanocrystals and explicitly stabilize the nanocrystal surface. The final concentrations only correspond to between 7% and 10% of the encapsulated API while at least 15% is in the form of MTNs. This indicates that MTNs do not directly translate into solubilized nanoparticles but rather serve as a starting point to improve solubility. To demonstrate the change in size after hydrolysis, the crystal size in solution is quantified by DLS. It is worth noting that the solution is centrifuged to remove residual cross-linked polymer and bulk crystals.

Crystals suspended in solution after hydrogel decomposition are always larger than the initial crystal sizes formed by the micellar domains of the hydrogels, as shown in Figure 6c. In all cases where MTNs were formed, two crystal sizes were observed in solution, ranging in size from 30 to 400 nm. In the case of surfactant S100, the smaller particle size in suspension is close to but still larger than the micelle hydrodynamic diameter. While this could represent the presence of "empty" micelles, the lack of any signal near the micelle size of any other surfactants and the large content of fenofibrate present in solution suggests that this contribution to the DLS signal is from surfactant stabilized FEN nanocrystals.

The apparent crystal growth upon hydration (from ≤10 to ≥25 nm) likely results from a combination of micelle swelling and Ostwald ripening. This is supported by the apparent linear correlation between the increase in API solubility with respect to the average hydrodynamic diameter of nanocrystals stabilized by surfactant, summarized in Figure 6d. Given that the majority of surfactant surrounds the MTNs, the larger crystals templated by the hydrogel mesh will predominantly coalesce and settle out of solution due to the lack of surfactant stabilization. In contrast, the smallest nanocrystals will dissolve the fastest and will quickly saturate the aqueous solution, as per the Noyes–Whitney and Ostwald–Freundlich equations, respectively. As shown in Figure 5, the MTNs are all smaller than the equilibrium micelle size of the surfactants. Thus, upon hydration the micelles will swell and destabilize the surface of the smallest crystals, further driving dissolution of the MTNs. Any crystals that remain stabilized in solution

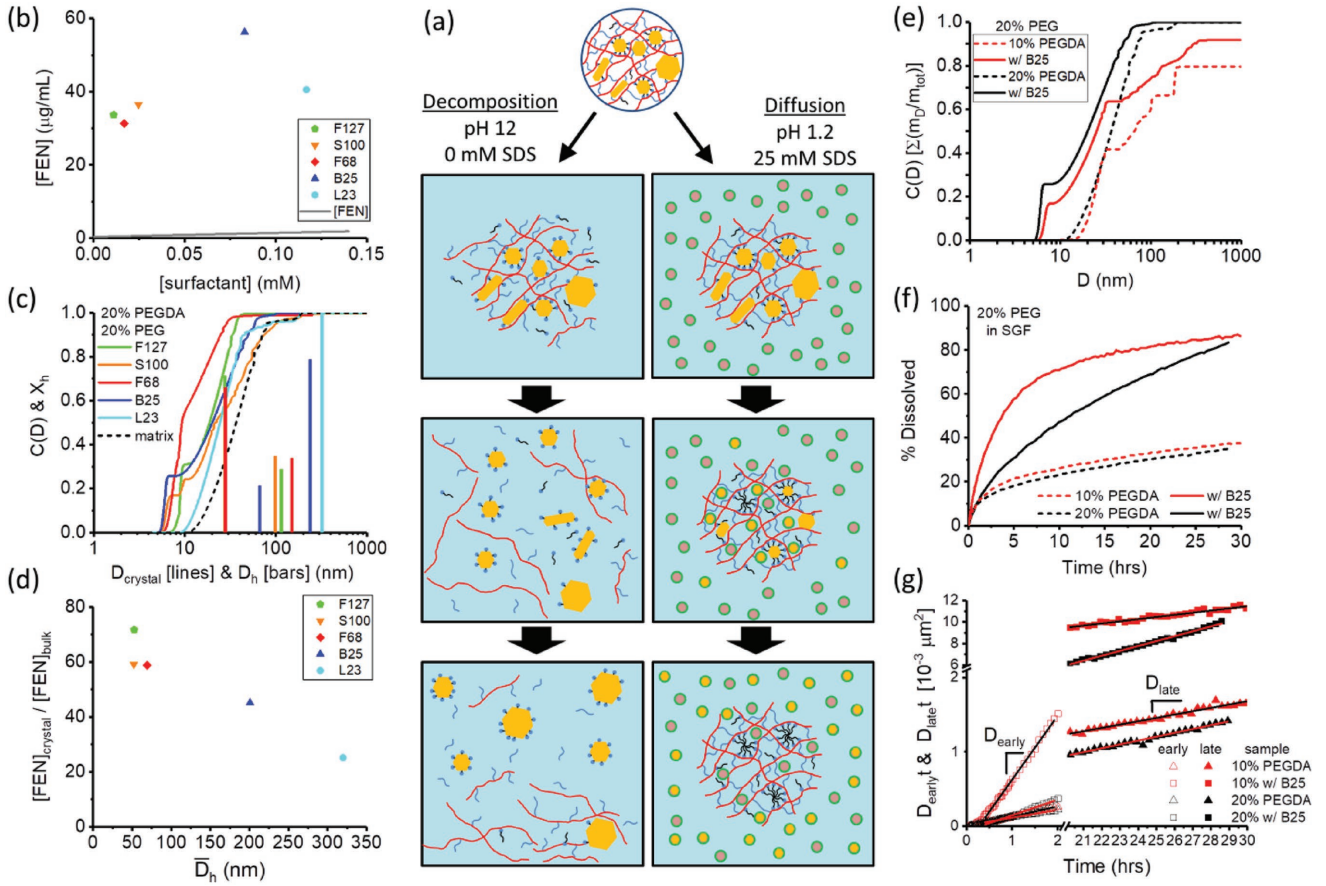

Figure 6. a) Schematic of drug release under alkaline decomposition conditions (left) yielding a saturated solution and acidic sink conditions (right). b) Concentrations of FEN in aqueous solution as a function of surfactant concentration obtained from UV–vis spectra of decomposed hydrogels loaded in FEN and various surfactants (colored symbols) compared with the FEN saturation concentration dependence on SDS concentration (line). c) The $C(D)$ functions (lines) of the decomposed FEN-loaded hydrogels compared with the hydrodynamic diameters, D_h, of solubilized nanocrystals measured by DLS (bars). d) The solubility enhancement of nanocrystalline FEN released from micelle-laden hydrogels relative to bulk FEN as a function of the effective hydrodynamic diameter of solubilized FEN crystals. e) The $C(D)$ functions of FEN-loaded hydrogels used in dissolution experiments. f) The dissolution profiles of micelle-laden hydrogel microparticles (500 μm in diameter) under sink conditions (pH 1.2, 25×10^{-3} M SDS). g) Scaling of early and late time mass transport from micelle-laden hydrogels to extract effective diffusion coefficients.

will then grow due to Ostwald ripening and absorb free surfactant to their surface. This proposed mechanism of growth will proceed until the reduced surface energy of nanocrystals can be stabilized by the surfactant and/or the total surface area of nanocrystals suspended in solution can be effectively coated by the corresponding content of surfactant released from the hydrogels. Importantly, the end result is that micelle-laden hydrogels can effectively enhance the solubility of fenofibrate from a final dosage form with minimal manufacturing steps and excipient content.

2.6. Characterization of Micelle-Templated Nanocrystal Dissolution Kinetics

Dissolution studies were carried out with simulated gastric fluid (SGF) to quantify the improvement in dissolution rate by MTNs. To ensure sink conditions are maintained, 25×10^{-3} M of SDS is added to the SGF to significantly increase the saturation concentration of fenofibrate in aqueous solution, following previously established protocol.[63,64] The acidic environment (pH = 1.2) hinders hydrolysis of PEGDA cross-linker ester groups composing the matrix. Thus, the hydrogel particles, which are 500 μm ± 75 μm in diameter, remain intact and drug release depends upon dissolution and diffusion of fenofibrate through the matrix into the bulk solution.

The $C(D)$ of two matrix PEGDA compositions, both with and without B25 surfactant, used in dissolution studies are provided in Figure 6e and the corresponding dissolution profiles are shown in Figure 6f. In the absence of surfactant, the CSDs of 10% and 20% PEGDA hydrogels are dominated by crystals ranging between 20–50 nm and 20–200 nm crystals, respectively. The corresponding release profiles indicate quick release of the first 15% of loaded fenofibrate, followed by drastically slower release to a cumulative total of 25%–30% after 24 h. In contrast, the addition of B25 surfactant yields a significant amount of MTNs at both PEGDA concentrations. These smaller crystals facilitate significantly faster initial dissolution and cumulative release close to 85% over 24 h. These release rates are significantly faster than prior dissolution experiments

Table 2. The effective diffusion coefficients of fenofibrate from hydrogels of 10% and 20% PEGDA, initially formed with 20% PEG, with either 0% or 8.4% B25 at early times (≤2 h), D_{early}, and late times (≥20 h), D_{late}. The diffusivity of fenofibrate in SDS micelles is reported[70] as 8.5×10^{-7} cm^2 s^{-1}.

%PEGDA	%B25	D_{early} [cm^2 s^{-1}]	D_{late} [cm^2 s^{-1}]
10	0	3.93×10^{-10}	1.27×10^{-10}
10	8.4	2.38×10^{-9}	6.05×10^{-10}
20	0	2.95×10^{-10}	1.44×10^{-10}
20	8.4	5.82×10^{-10}	1.26×10^{-9}

of hydrophobic drug from nondegrading hydrogels, which are reported to take several days to a week for 50% release,[44] but still slower than fast-degrading, ionically cross-linked hydrogels with sub-micrometer crystals.[63,64,66] However, while the 20% PEGDA matrix with B25 has a higher quantity of MTNs, the 10% PEGDA matrix with B25 releases more fenofibrate within the first 24 h. These results highlight the fact that drug release is a balance of crystal size (i.e., dissolution rate) and mesh size (i.e., diffusion rate). As a side note, swelling is not a major factor influencing the release kinetics. The matrix swells rapidly within 5 min and reaches its fully swollen state within an hour, as quantified by swelling experiments (shown in the Supporting Information).

The solute diffusion coefficient through the matrix is a strong function of the mesh size,[45] which is smaller in the 20% PEGDA matrix. Models of mass transport from hydrogels can be used to extract the effective diffusion coefficient of API at early (first 2 h) and late (last 10 h) times according to a previously described power law of order 0.5 and an exponential function, respectively.[72] The corresponding fits to each hydrogel are summarized in **Table 2**. The effective diffusion coefficients are significantly slower than the free fenofibrate in solution, indicative of the influence of the hydrogel mesh. However, the diffusivity of API from hydrogels is significantly improved in the presence of B25 and correspondingly MTNs. At early times, the fast dissolution of MTNs improves effective mass transport by a factor of 6 and 2 in 10% and 20% PEGDA hydrogels, respectively. The smaller improvement in 20% PEGDA hydrogels is representative of the smaller mesh size that hinders diffusion directly and indirectly by more rapidly reaching the saturation concentration in the more confined environment. At longer times, the B25 yields a factor of 4.8 and 8.7 improvement in effective diffusivity in 10% and 20% PEGDA hydrogels, respectively. Thus, the overall smaller distribution of crystal sizes in hydrogels with 20% PEGDA and B25 surfactant sustains, and appears to improve, the release of API over time. Thus, while the diffusivity is hindered by a smaller mesh size, MTNs provide a significant improvement in the effective rate of API release from micelle-laden hydrogels.

As a final note, micelle-laden hydrogels include additional beneficial features for effective delivery of hydrophobic APIs. For example, the products of PEGDA hydrolysis such as cross-linked polyacrylate are similar to commercially available excipients, such as Eudragit and Carbopol. These materials have been found to have gastroretentive and mucoadhesive properties,[73–75] which can broaden the therapeutic benefit of these hydrogels. The formation of surfactant stabilized nanocrystals on the order of 30 nm after release from the hydrogel may improve API performance by preventing premature metabolism and clearance by the kidneys that occurs with smaller nanomaterials (≤10 nm crystals). Therefore, these hydrogels may also prevent fast clearance of hydrophobic drugs while enhancing solubility. Other studies have also identified higher permeability of nanoparticles through the cell wall of the gastrointestinal (GI) tract, especially those "masked" by PEG grafting on the surface.[76] Cross-linked polyacrylate is a by-product during degradation and may also provide some bioadhesion to increase the residence time in the GI tract and offer a route to design controlled release OSD forms.[77] While future studies on micelle-laden hydrogels are necessary to confirm this hypothesis, it is reasonable to believe that these materials also have the ability to increase permeability and therefore, significantly enhance the bioavailability of orally delivered hydrophobic drugs. Lastly, to facilitate the use of micelle-laden hydrogels as OSDs, additional work is ongoing to design cross-linking functionalities that rapidly degrade in physiologically relevant solutions.

3. Conclusions

We have demonstrated the ability to integrate surfactant micelles into PEGDA-based hydrogel scaffolds to serve as domains for the formation of hydrophobic API nanocrystals. The model hydrophobic drug, fenofibrate, was used for its available calibration curve comparing crystal size to melting temperature in order to identify the distribution of crystal sizes formed in micelle-laden hydrogels. Nanocrystals ranging from 10 to 400 nm were found to form in "plain" hydrogels without surfactant present. The addition of surfactant in the form of micelles provided hydrophobic domains that successfully templated the formation of nanocrystals as small as 4 nm in size. A 16 carbon (cetyl) chain was found to be the minimum size of the hydrophobic segment of the surfactant to reliably induce crystallization of the hydrophobic API studied. Importantly, the crystal size formed in micelles is independent of hydrogel chemistry and mesh size. As a result, micelle-laden hydrogels drastically simplify the production of nanocrystalline OSDs and provide versatility in customizing the release profile. The loading of API in these micelle-laden hydrogels can reach up to 90% by mass and can improve solubility by up to a factor of 70. Under all conditions, the presence of surfactant also stabilized nanocrystals between 30 and 400 nm after decomposition of the hydrogel. Therefore, micelle-laden hydrogels are a promising platform technology as an OSD to increase the solubility and dissolution of hydrophobic APIs, although further work is necessary to facilitate disintegration and release in physiologically relevant media.

4. Experimental Section

Materials: All chemicals were purchased from Sigma-Aldrich and used as received. The chemical constituents used in the synthesis, washing, and loading of micelle-laden hydrogels include ethanol, ethyl acetate, FEN, 2-hydroxy-2-methylpropiophenone [PI], PEG (M_n = 200 g mol^{-1}),

PEGDA (M_n = 700 g mol^{-1}), and poly(ethylene glycol) behenyl ether methacrylate [B25] solution (M_n = 1500 g mol^{-1}). Additional surfactants include Brij C10 [C10], Brij 58 [C20], decaethylene glycol monododecyl ether [L10], Brij L23 [L23], Brij S20 [S20], Brij S100 [S100], Pluronic F-68 [F68], and Pluronic F-127 [F127]. The reactants used to synthesize acrylated surfactants include dichloromethane (DCM), acryloyl chloride, and sodium bicarbonate.

Synthesis of Acrylated Surfactants: All acrylated surfactants other than B25 were synthesized by acylation of commercially available alkyl ethoxy and poloxamer surfactants. The reaction procedure of prior studies was used,[78] which were carried out at room temperature using an Erlenmeyer flask on a stir plate. Surfactant (20 mmol) was first solubilized in DCM (120 mL) under gentle stirring before adding a 20% molar excess of sodium bicarbonate. An identical molar excess quantity of acryloyl chloride was added to DCM (20 mL), which was then added dropwise to the surfactant mixture under gentle stirring. The reaction was carried out overnight (18–24 h). The mixture was filtered through a Buchner funnel to remove solids then the solvent was removed under vacuum at 30 °C. The resulting structures of modified alkyl ethoxy and poloxamer surfactants were monoacrylate and diacrylate molecules, respectively. The surfactants and reaction products were characterized by FTIR spectroscopy with a Smiths IdentifyIR spectrometer.

Hydrogel Synthesis and Loading: Hydrogels were formed by first mixing all precursor components (water, PEG, PEGDA, PI, and acrylated surfactant) into a homogeneous solution. Tablets were formed by filling a 14 mm diameter by 7 mm height cylindrical polypropylene mold with precursor solution (1 mL) and then exposing it to a UV lamp (365 nm, 1.3 W) for 5 min to fully cross-link the material. Microparticles were generated with an Upchurch Scientific PEEK MicroCross microfluidic cross-junction with 1/16 in. outer diameter tubing. The precursor solution was flowed through the central inlet as the dispersed phase and mineral oil was flowed through the two tangential inlets as the continuous phase to create 500 ± 75 µm diameter droplets of precursor solution. While flowing through the outlet tubing, the droplets were exposed to the same UV lamp for 5 min to cross-link before being separated from the oil. After cross-linking, unreacted PEGDA and surfactant and PI and PEG were removed by soaking tablet and microparticle hydrogels in fresh ethanol three times for 8–24 h followed by soaking in fresh ethyl acetate three times for 8–24 h before being loaded with fenofibrate. Drug loading was carried out by transferring the washed hydrogels from ethyl acetate into a solution of fenofibrate in ethyl acetate (450 mg mL^{-1}). Hydrogels were soaked in FEN solution for 8–24 h to ensure complete homogeneous loading of FEN. Crystallization was induced by transferring FEN-soaked hydrogels to a vacuum oven at 80 °C and roughly 0.1 MPa pressure and allowing the ethyl acetate solvent to evaporate overnight (18–24 h) to ensure complete drying of the hydrogel.

Experimental Characterization of Nanocrystals: The crystalline FEN within hydrogels was characterized by X-ray diffraction (XRD) and DSC to confirm the polymorph of the crystal and the crystal size, respectively. XRD experiments were carried out on a PANalytical XPert Pro with a 4° aperture and 0.5° slit using a continuous scanning detector ranging from a 2θ angle of 4°–40° with a scan rate of 1° min^{-1}. DSC experiments were conducted on a TA Instruments Q2000 with aluminum Tzero pans using a protocol that first equilibrated at −20 °C before ramping the temperature at a rate of 10 °C min^{-1} to a maximum of 180 °C. Previously published data[25] relating the melting point to crystal size were used as a calibration curve to quantify a crystal size distribution in each hydrogel. The calibration curves are provided in the Supporting Information. The drug loading of hydrogels with FEN was quantified by integration of DSC curves and confirmed in certain samples by measurement with TGA. TGA experiments were run on a TA instruments Q5000. Samples were first equilibrated at 40 °C then heated at 10 °C min^{-1} to 500 °C.

Modeling of Crystal Size Distribution: Each DSC thermogram was a result of a unique distribution of crystal sizes formed within a hydrogel. The relative mass of each crystal size could be obtained by reproducing the experimental thermogram as a summation of peaks representing a given size. A correlation curve was used to quantify crystal size from the FEN melting point according to the Gibbs–Thompson equation

$$T_{m,p} = T_{m,b}\left(1 - 4V_m\frac{C_T}{D}\right) \quad (1)$$

where $T_{m,p}$ is the particle melting point, $T_{m,b}$ is the bulk melting point, V_m is the molar volume, D is the particle diameter, and C_T is the Turnbull coefficient, defined here as

$$C_T = \gamma_{SL}/\Delta H_m \approx \text{constant} \quad (2)$$

where γ_{SL} is the solid–liquid surface energy and ΔH_m is the enthalpy of melting. The Turnbull coefficient is shown to be constant for a given substance,[68] which is what yields a linear relationship between $T_{m,p}$ and $1/D$ and also suggests a direct connection between ΔH_m and γ_{SL}. Theoretical work represents ΔH_m as a polynomial expansion in terms of γ_{SL}. Herein, the dependence of ΔH_m on $1/D$ is represented as an exponential function given the similarity of the exponential Taylor series summation to the proposed polynomial expansion and the unphysical negative value for ΔH_m at small particle sizes when using a linear function.[25] The best fit functions to the data set from ref. [25] are $T_{m,p} = 81.628 - 344.83/D$ in units of °C and $\Delta H_m(D) = 90.632\exp(-8.594/D)$ in units of J g^{-1} where crystal size is in units of nanometer (with R^2 values of 0.987 and 0.983, respectively).

A fitting algorithm was written in MATLAB to reproduce the experimental DSC thermogram as a summation of Gaussian peaks. Before conducting a nonlinear least squared minimization fit, the background component of each signal was removed. To remove noise in the data, the raw signal was fit to a spline function. The background was identified by the slope of the spline curve according to $(dH/dT) \leq 0.0035\ W/K$ as well as creating linear interpolations between troughs of adjacent peaks. A representative result of this background subtraction is presented in the Supporting Information.

Individual crystal peaks were represented by a Gaussian function where the magnitude was used as a fitting variable and the width was held constant. A physically representative peak width was determined by fitting a (background subtracted) DSC thermogram of a bulk fenofibrate sample. The initial input was a single peak at the temperature of the maximum in the data set.

The mass of each crystal size, $m(D)$, was determined by first integrating an individual peak area and dividing by the heating rate, $\dot{T}$, and enthalpy of melting, $\Delta H(D)$, for the crystal size corresponding to the peak

$$m(D) = \frac{\int_{-\infty}^{\infty} I(D,T'')\,dT''}{\dot{T}\,\Delta H(D)} \quad (3)$$

The total mass of all crystals, m_{total}, within the hydrogel was determined by the sum of all peaks

$$m_{total} = \sum_{i=1}^{\infty} m(D_i) \quad (4)$$

Dividing m_{total} by the total sample mass produced an estimate of the loaded weight fraction of fenofibrate. Dividing the mass of a given crystal size by the total mass of fenofibrate yielded the mass fraction of each crystal size, X_D. The cumulative crystal size distribution, which quantifies the mass fraction of crystals below or equal to a given size, was determined by

$$C(D) = \sum_{D''=0}^{D} m(D'')/m_{total} \quad (5)$$

The sequence of steps used to extract a cumulative crystal size distribution from DSC data is illustrated in the Supporting Information.

Characterization of Drug Release Kinetics: Properties of FEN nanocrystals during and after release from micelle-laden hydrogels into suspension in aqueous media were characterized by two different methods. First, microparticles (500 µm diameter) of fenofibrate loaded

hydrogels were suspended in simulated gastric fluid (50×10^{-3} M sodium phosphate, 1.0 M HCl, 25×10^{-3} M SDS, 600 mL) in a Varian VK7025 USP Type II dissolution apparatus at 37 °C with a paddle stirring at 75 RPM. Automated concentration measurements were taken using a Varian Cary 50Bio UV–Vis spectrophotometer at 290 nm with a 10 mm path length probe. The effective diffusion coefficients of API at early, D_{early}, and late, D_{late}, times were extracted using previously developed mass transport models from hydrogels.[72] The scaling for diffusion at early times is as follows

$$D_{early}t = (\pi/16)(X\delta)^2 \quad (6)$$

and that for diffusion at late times is as follows

$$D_{late}t = \ln\left[(1-X)\pi^2/8\right](\delta/\pi)^2 \quad (7)$$

where X is the fraction of drug dissolved and $\delta = 250$ µm, which is the characteristic lengthscale of diffusion defined as the radius of the hydrogel microparticles. Second, nanocrystals were released by decomposing the hydrogel matrix (20 mg) in a sodium hydroxide solution (1.0 M, 20 mL) overnight at room temperature with gentle stirring. The solution was then left for an additional day without stirring to allow matrix residue to settle, leaving behind a clear suspension of nanocrystals. The crystal size distributions were quantified with a Brookhaven Instruments NanoBrook 90Plus DLS instrument by fitting the measured correlation functions with a double exponential function to quantify hydrodynamic diameters. The concentration of fenofibrate after release was quantified using UV–vis absorbance at a wavelength of 290 nm. A calibration curve of UV–vis intensity to FEN concentration was produced in aqueous solutions of SDS (25×10^{-3} M) with a range of concentrations (1–100 µg mL^{-1}) well below the saturation concentration (193 µg mL^{-1}).

Supporting Information

Supporting Information is available from the Wiley Online Library or from the author.

Acknowledgements

The manuscript was written through contributions of all authors. All authors have given approval to the final version of the manuscript. This work was funded in part by support from Merck & Co. as well as funding from the Singapore National Research Foundation through an Intra-CREATE grant.

Conflict of Interest

The authors declare no conflict of interest.

Keywords

hydrogels, hydrophobic drugs, micelles, nanocrystals, solubility

Received: August 21, 2018
Revised: November 17, 2018
Published online:

[1] M. W. Tibbitt, J. E. Dahlman, R. Langer, *J. Am. Chem. Soc.* **2016**, *138*, 704.
[2] V. Wagner, A. Dullaart, A.-K. Bock, A. Zweck, *Nat. Biotechnol.* **2006**, *24*, 1211.
[3] H. Dolgos, M. Trusheim, D. Gross, J. P. Halle, J. Ogden, B. Osterwalder, E. Sedman, L. Rossetti, *Drug Discovery Today* **2016**, *21*, 517.
[4] L. Gao, G. Liu, J. Ma, X. Wang, L. Zhou, X. Li, *J. Controlled Release* **2012**, *160*, 418.
[5] S. Shen, Y. Wu, Y. Liu, D. Wu, *Int. J. Nanomed.* **2017**, *12*, 4085.
[6] H. R. Lakkireddy, D. Bazile, *Adv. Drug Delivery Rev.* **2016**, *107*, 289.
[7] S. Kalepu, V. Nekkanti, *Acta Pharm. Sin. B* **2015**, *5*, 442.
[8] A. M. Thayer, *Chem. Eng. News* **2010**, *88*, 13.
[9] M. S. Ku, *AAPS J.* **2008**, *10*, 208.
[10] C. Lipinski, *Am. Pharm. Rev.* **2002**, *5*, 82.
[11] L. Z. Benet, F. Broccatelli, T. I. Oprea, *AAPS J.* **2011**, *13*, 519.
[12] L. Di, P. V. Fish, T. Mano, *Drug Discovery Today* **2012**, *17*, 486.
[13] S. Stegemann, F. Leveiller, D. Franchi, H. de Jong, H. Lindén, *Eur. J. Pharm. Sci.* **2007**, *31*, 249.
[14] H. Havel, G. Finch, P. Strode, M. Wolfgang, S. Zale, I. Bobe, H. Youssoufian, M. Peterson, M. Liu, *AAPS J.* **2016**, *18*, 1373.
[15] H. A. Havel, *AAPS J.* **2016**, *18*, 1351.
[16] B. Tang, G. Cheng, J. C. Gu, C. H. Xu, *Drug Discovery Today* **2008**, *13*, 606.
[17] T. Gershanik, S. Benita, *Eur. J. Pharm. Biopharm.* **2000**, *50*, 179.
[18] T. Loftsson, M. E. Brewster, *J. Pharm. Pharmacol.* **2010**, *62*, 1607.
[19] P. P. Constantinides, *Pharm. Res.* **1995**, *12*, 1561.
[20] J. A. Kramer, J. E. Sagartz, D. L. Morris, *Nat. Rev. Drug Discovery* **2007**, *6*, 636.
[21] W. W. L. Chin, J. Parmentier, M. Widzinski, E. N. H. Tan, R. Gokhale, *J. Pharm. Sci.* **2014**, *103*, 2980.
[22] R. Shegokar, R. H. Müller, *Int. J. Pharm.* **2010**, *399*, 129.
[23] B. E. Rabinow, *Nat. Rev. Drug Discovery* **2004**, *3*, 785.
[24] N. J. Babu, A. Nangia, *Cryst. Growth Des.* **2011**, *11*, 2662.
[25] L. M. Dwyer, V. K. Michaelis, M. O'Mahony, R. G. Griffin, A. S. Myerson, *CrystEngComm* **2015**, *17*, 7922.
[26] D. Singhal, W. Curatolo, *Adv. Drug Delivery Rev.* **2004**, *56*, 335.
[27] K. Kawakami, *Adv. Drug Delivery Rev.* **2012**, *64*, 480.
[28] T. Van Duong, G. Van den Mooter, *Expert Opin. Drug Delivery* **2016**, *13*, 1.
[29] E. Merisko-Liversidge, G. G. Liversidge, *Adv. Drug Delivery Rev.* **2011**, *63*, 427.
[30] J. P. Möschwitzer, *Int. J. Pharm.* **2013**, *453*, 142.
[31] J. U. A. H. Junghanns, R. H. Müller, *Int. J. Nanomed.* **2008**, *3*, 295.
[32] D. A. Shah, S. B. Murdande, R. H. Dave, *J. Pharm. Sci.* **2016**, *105*, 10.
[33] S. B. Murdande, D. A. Shah, R. H. Dave, *J. Pharm. Sci.* **2015**, *104*, 2094.
[34] L. Osterberg, T. Blaschke, *N. Engl. J. Med.* **2005**, *353*, 487.
[35] A. Shahiwala, *Expert Opin. Drug Delivery* **2011**, *8*, 1521.
[36] R. Lipp, *Am. Pharm. Rev.* **2013**, *16*, 1.
[37] M. V. Chaubal, *Drug Discovery Today* **2004**, *9*, 603.
[38] M. Hariharan, L. D. Ganorkar, G. E. Amidon, A. Cavallo, P. Gatti, M. J. Hageman, I. Choo, J. L. Miller, U. J. Shah, *Pharm. Technol.* **2003**, *27*, 68.
[39] M. P. Gleeson, A. Hersey, D. Montanari, J. Overington, *Nat. Rev. Drug Discovery* **2011**, *10*, 197.
[40] Y. Qiu, X. Li, J. Z. Duan, *J. Pharm. Sci.* **2014**, *103*, 507.
[41] H. Valo, S. Arola, P. Laaksonen, M. Torkkeli, L. Peltonen, M. B. Linder, R. Serimaa, S. Kuga, J. Hirvonen, T. Laaksonen, *Eur. J. Pharm. Sci.* **2013**, *50*, 69.
[42] E. Kwong, J. Higgins, A. C. Templeton, *Int. J. Pharm.* **2011**, *412*, 1.
[43] S. M. Paul, D. S. Mytelka, C. T. Dunwiddie, C. C. Persinger, B. H. Munos, S. R. Lindborg, A. L. Schacht, *Nat. Rev. Drug Discovery* **2010**, *9*, 203.
[44] J. Li, D. J. Mooney, *Nat. Rev. Mater.* **2016**, *1*, 16071.
[45] N. A. Peppas, P. Bures, W. Leobandung, H. Ichikawa, *Eur. J. Pharm. Biopharm.* **2000**, *50*, 27.
[46] T. R. Hoare, D. S. Kohane, *Polymer* **2008**, *49*, 1993.

[47] Y. Qiu, K. Park, *Adv. Drug Delivery Rev.* **2012**, *64*, 49.
[48] N. A. Peppas, A. Khademhosseini, *Nature* **2016**, *540*, 335.
[49] R. M. Ottenbrite, K. Park, T. Okano, *Biomedical Applications of Hydrogels Handbook*, Springer, **2010**.
[50] Y. Diao, M. E. Helgeson, A. S. Myerson, T. A. Hatton, P. S. Doyle, B. L. Trout, *J. Am. Chem. Soc.* **2011**, *133*, 3756.
[51] Y. Diao, M. E. Helgeson, Z. A. Siam, P. S. Doyle, A. S. Myerson, T. A. Hatton, B. L. Trout, *Cryst. Growth Des.* **2012**, *12*, 508.
[52] Y. Wang, Y. Zheng, L. Zhang, Q. Wang, D. Zhang, *J. Controlled Release* **2013**, *172*, 1126.
[53] A. Tuomela, J. Hirvonen, L. Peltonen, *Pharmaceutics* **2016**, *8*, 16.
[54] D. Gu, A. J. O'Connor, G. G. H. Qiao, K. Ladewig, *Expert Opin. Drug Delivery* **2017**, *14*, 879.
[55] U. Kedar, P. Phutane, S. Shidhaye, V. Kadam, *Nanomedicine* **2010**, *6*, 714.
[56] H. J. Chung, T. G. Park, *Nano Today* **2009**, *4*, 429.
[57] L. Bromberg, *Expert Opin. Drug Delivery* **2005**, *2*, 1003.
[58] M. T. Calejo, S. A. Sande, B. Nyström, *Expert Opin. Drug Delivery* **2013**, *10*, 1669.
[59] D. Mawad, J. L. J. R. Foster, A. Lauto, *Int. J. Pharm.* **2008**, *360*, 231.
[60] J. Y. Kim, W. Il Choi, Y. H. Kim, G. Tae, S. Y. Lee, K. Kim, I. C. Kwon, *J. Controlled Release* **2010**, *147*, 109.
[61] M. Vandenhaute, J. Schelfhout, S. Van Vlierberghe, E. Mendes, P. Dubruel, *Eur. Polym. J.* **2014**, *53*, 126.
[62] J. B. Lee, J. J. Yoon, D. S. Lee, T. G. Park, *J. Biomater. Sci., Polym. Ed.* **2004**, *15*, 1571.
[63] A. Z. M. Badruddoza, P. D. Godfrin, A. S. Myerson, B. L. Trout, P. S. Doyle, *Adv. Healthcare Mater.* **2016**, *5*, 1960.
[64] H. B. Eral, M. O'Mahony, R. Shaw, B. L. Trout, A. S. Myerson, P. S. Doyle, *Chem. Mater.* **2014**, *26*, 6213.
[65] A. Gupta, H. B. Eral, T. A. Hatton, P. S. Doyle, *Soft Matter* **2016**, *12*, 2826.
[66] H. B. Eral, V. López-Mejías, M. O'Mahony, B. L. Trout, A. S. Myerson, P. S. Doyle, *Cryst. Growth Des.* **2014**, *14*, 2073.
[67] A. K. Patri, M. A. Dobrovolskaia, S. T. Stern, S. E. McNeil, *Nanotechnology for Cancer Therapy*, Taylor & Francis Group **2007**, pp. 105–137.
[68] S. Shimizu, K. V. Agrawal, M. O'Mahony, L. W. Drahushuk, N. Manohar, A. S. Myerson, M. S. Strano, *Langmuir* **2015**, *31*, 10113.
[69] D. Missirlis, J. A. Hubbell, N. Tirelli, *Soft Matter* **2006**, *2*, 1067.
[70] G. E. Granero, C. Ramachandran, G. L. Amidon, *Drug Dev. Ind. Pharm.* **2005**, *31*, 917.
[71] P. A. Bhat, A. A. Dar, G. M. Rather, *J. Chem. Eng. Data* **2008**, *53*, 1271.
[72] L. Serra, J. Doménech, N. A. Peppas, *Biomaterials* **2006**, *27*, 5440.
[73] V. Grabovac, D. Guggi, A. Bernkop-Schnürch, *Adv. Drug Delivery Rev.* **2005**, *57*, 1713.
[74] J. D. Smart, *Adv. Drug Delivery Rev.* **2005**, *57*, 1556.
[75] A. Sosnik, J. Das Neves, B. Sarmento, *Prog. Polym. Sci.* **2014**, *39*, 2030.
[76] H. Liu, L. S. Taylor, K. J. Edgar, *Polymer* **2015**, *77*, 399.
[77] G. P. Andrews, T. P. Laverty, D. S. Jones, *Eur. J. Pharm. Biopharm.* **2009**, *71*, 505.
[78] P. Ferguson, D. C. Sherrington, A. Gough, *Polymer* **1993**, *34*, 3281.

